The adsorption and decomposition of SF_6 over defective and hydroxylated MgO surfaces : a DFT study

Reference:
Cui Zhaolun, Hao Yanpeng, Jafarzadeh Amin, Li Shangkun, Bogaerts Annemie, Li Licheng.- The adsorption and decomposition of SF_6 over defective and hydroxylated MgO surfaces : a DFT study
Surfaces and interfaces - ISSN 2468-0230 - 36(2023), 102602
Full text (Publisher's DOI): https://doi.org/10.1016/J.SURFIN.2022.102602
To cite this reference: https://hdl.handle.net/10067/1943640151162165141

The adsorption and decomposition of SF_6 over defective and hydroxylated MgO surfaces: A DFT study

Zhaolun Cui[a], Yanpeng Hao[a], Amin Jafarzadeh[b], Shangkun Li[b], Annemie Bogaerts[b], Licheng Li[a]*

[a]School of Electric Power Engineering, South China University of Technology, Guangzhou 510630, China

[b]Research group PLASMANT, Department of Chemistry, University of Antwerp, Universiteitsplein 1, BE-2610 Wilrijk-Antwerp, Belgium

Abstract: Plasma degradation is one of the most effective methods for the abatement of greenhouse gas sulfur hexafluoride (SF_6). To evaluate the potential of MgO as a catalyst in plasma degradation, we investigate the catalytic properties of MgO on SF_6 adsorption and activation by density functional theory (DFT) where the O-defective and hydroxylated surfaces are considered as two typical plasma-generated surfaces. Our results show that perfect MgO (001) and (111) surfaces cannot interact with SF_6 and only physical adsorption happens. In case of O-defective MgO surfaces, the O vacancy is the most stable adsorption site. SF_6 undergoes a decomposition to SF_5 and F over the O-defective MgO (001) surface and undergoes an elongation of the bottom S-F bond over the O-defective (111) surface. Besides, SF_6 shows a physically adsorption at the stepsite of the MgO (001) surface, accompanied by small changes in its bond angle and length. Furthermore, SF_6 is found to be physically and chemically adsorbed over 0.5 and 1.0 ML (monolayer) H-covered O-terminated MgO (111) surfaces, respectively. The SF_6 molecule undergoes a self-decomposition on the 1.0 ML hydroxylated surface via a surface bonding process. This study shows that defective and hydroxylated MgO surfaces have the surface capacities for SF_6 activation, which shows that MgO has potential as packing material in SF_6 waste treatment in packed-bed plasmas.

Keywords: SF_6, MgO, surface property, adsorption, DFT

1 Introduction

In recent decades, SF_6 has been widely used in the power industry as a dielectric gas, due to its excellent properties on insulation and arc extinction [1]. However, SF_6 is a greenhouse gas and is listed as one of the restricted emission gases in the Kyoto protocol [2]. The global warming potential of SF_6 is 23500 times that of CO_2 [3]. Therefore, its increasing use and emission cause great threats to the atmospheric environment.

Since the end of last century, great efforts have been made on SF_6 abatement. The most used method is thermal degradation, where SF_6 is decomposed and reacts with CaO or $Ca(OH)_2$ in a 1100° C furnace[1]. However, the maintenance of high temperature and the overload of alkaline solids leads to high energy consumption. By adding metallic phosphate or metallic oxide, the degradation temperature of SF_6 can be lowered to 600~900 K, gaining a better energy efficiency, but the degradation rate is limited [4, 5]. Besides, researchers found that non-thermal plasma (NTP) holds promise for SF_6 abatement, by means of dielectric barrier discharges (DBD), micro-discharges, radio-frequency discharges, and so on [6]. In NTP treatment, the SF_6 molecules can be effectively degraded at atmospheric temperature and pressure, but toxic gas products like SO_2F_2, SO_2, and HF are generated. The addition of metal oxide like Al_2O_3 in NTP, typically as a packing material in a

so-called packed bed DBD, improves the degradation of SF_6 and regulates its reaction pathway [7, 8]. In 2020, Yael et. al. achieved a sustainable and tunable degradation of SF_6 by a Mg/MgO plasmon-catalytic system, where the S and F elements are fixed as MgF_2 and $MgSO_4$, respectively. The reacted Mg products can then be reduced by hydrogen plasma for reuse [9]. Although the degradation rate is limited in the above study, it shows the potential of MgO for SF_6 catalytic degradation. In a plasma-catalytic system, the plasma discharge has significant impact on the packing material surface, thus affecting the surface reactions [10, 11]. For instance, during a thermal or a NTP-based degradation of SF_6, O_2, H_2O and H_2 are often added as reactive gases to promote the degradation and regulate the product distribution [12, 13]. MgO therefore could be affected from the gas environment to form O-terminated surfaces in O-rich conditions and get hydroxylated by H species [14, 15]. To further evaluate the catalytic property of MgO and whether it can be integrated with other technologies, such as thermal catalysis and plasma catalysis (i.e., as packing material in packed bed DBD plasmas), the interaction between SF_6 and MgO should be carefully investigated.

In this work, we carried out a density functional theory (DFT) study on the adsorption and the decomposition of SF_6 over MgO surfaces. The (001) and O-terminated (111) surfaces are selected as the typical MgO surfaces since they have been entensively studied in previous works as the representitive catalytic surfaces [16, 17]. The O vacancy, stepsite and H coverage are taken into consideration to better describe the surface conditions that correspond to the actual MgO materials in plasma-catalysis. Charge analysis is carried out to uncover the bonding and the charge transfer processes between the SF_6 molecules and the MgO surfaces. The results reveal that chemical adsorption only happens over special sites, like O vacancies and H-covered surfaces. Our study demonstrates that MgO is a potential catalyst or packing material for SF_6 degradation in NTP abatement.

2 Computational details

The DFT calculations are carried out by the CP2K/Quickstep package [18]. The generalized gradient approximation of Perdew-Burke-Ernzerhof functional is applied to describe the exchange-correlation terms [19]. The DFT-D3 method is used for the dispersion correction [20]. The Goedecker–Teter–Hutter (GTH) pseudopotentials are applied to describe the core electrons [21], and the Gaussian and plane wave method (GPW) is applied, with a plane wave cutoff to be 800 Ry [22]. The molecularly optimized double-ζ polarized basis sets (m-DZVP) are applied for the expansion of the wave functions. Bader analysis is used to describe the charge transfer process [23].

The (001) and O-terminated (111) MgO slab models are built, as shown in Fig. S1. Both slabs have five layers and the bottom two layers are fixed during the calculation. The XY dimensions are 11.91×11.91 Å for both slabs and a vacuum layer of 30 Å is applied to avoid periodic interactions. The O vacancy is made by removing one of the O surface atoms from the (001) and (111) surface, as shown in Fig. S2 [24, 25]. The step site of the MgO (001) slab is made according the Ref. [26], where the atoms in the right part of the surface layer are removed and the edge composed of O atoms is exposed. The O-terminated MgO (111) surfaces with H coverages of 50% or 100% (labelled to be 0.5 and 1.0 ML) are made according to Ref. [27] to simulate the hydration effects of the MgO material, as shown in Fig. S3. During the calculation, the surface dipole correction is applied for the MgO (111) surfaces.

The adsorption energy E_{ad} of gas molecules on the MgO surface is calculated by Eq (1).

$$E_{ad} = E_{gas+slab} - E_{gas} - E_{slab} \quad (1)$$

Where E_{gas} and E_{slab} are the energies of gas molecules and of the MgO slabs, respectively, and $E_{gas+slab}$ is the total energy of the adsorbed system. A more negative E_{ad} corresponds to a more stable adsorption.

3 Results and discussion

3.1 SF_6 adsorption on perfect MgO (001) and (111) surfaces

The stable adsorption configurations of SF_6 over perfect MgO (001) and (111) surfaces are calculated, as shown in Fig.1 and Fig.2. For each site, two kinds of initial configurations are considered, one of them is the S-F bond set perpendicular to the surface, and the other is the two bottom F atoms parallel to the surface. The configuration with a more negative E_{ad} is considered to be the stable one. The adsorption energies E_{ad} and the distance between SF_6 and the slab surface are summarized in Table 1. In Fig.1 and Fig.2, there is no chemical bonding made between the SF_6 molecule and the MgO surfaces. At the same time, the SF_6 molecule structure has no obvious change after the adsorption and this indicates that only physical adsorptions happen. The E_{ad} of SF_6 at Mg, O and the hollow sites over the MgO (001) surface are all the same, i.e., -0.21 eV, while SF_6 adsorbing at the hollow site has the smallest adsorption distance of 2.45 Å. By contrast, over the MgO (111) surface, the most stable adsorption shows up at the hollow site, with the highest E_{ad} to be -0.23 eV. However, SF_6 adsorbing at the hollow site shows the largest adsorption distance to be 2.71 Å. The smallest adsorption distance shows up at the Mg site, with E_{ad} to be only -0.16 eV. These results indicate that the interaction between the SF_6 molecule and the perfect MgO surfaces is very weak and the adsorption process is mainly induced by the Van der Waals forces.

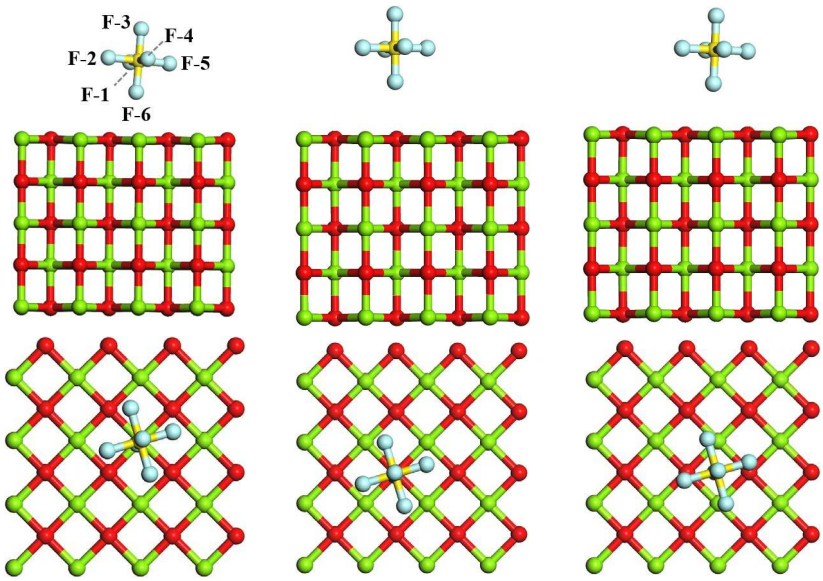

(a) Mg (b) O (c) Hollow

Fig. 1 Adsorption configurations of SF_6 over the perfect MgO (001) surface, in side view (upper panels) and top view (lower panels). Green, red, yellow and blue balls are Mg, O, S and F atoms, respectively.

Table 1 Adsorption energy and distance of SF_6 over perfect MgO (001) and (111) surfaces

Adsorption site	MgO (001)		MgO (111)	
	E_{ad} (eV)	Adsorption distance[a] (Å)	E_{ad} (eV)	Adsorption distance[a] (Å)

Mg	-0.21	2.51	-0.16	2.21
O	-0.21	2.80	-0.20	2.51
Hollow	-0.21	2.83	-0.23	2.68

[a]This corresponds to the distance between the bottom F atom in SF_6 and the closest surface atom on the MgO surface.

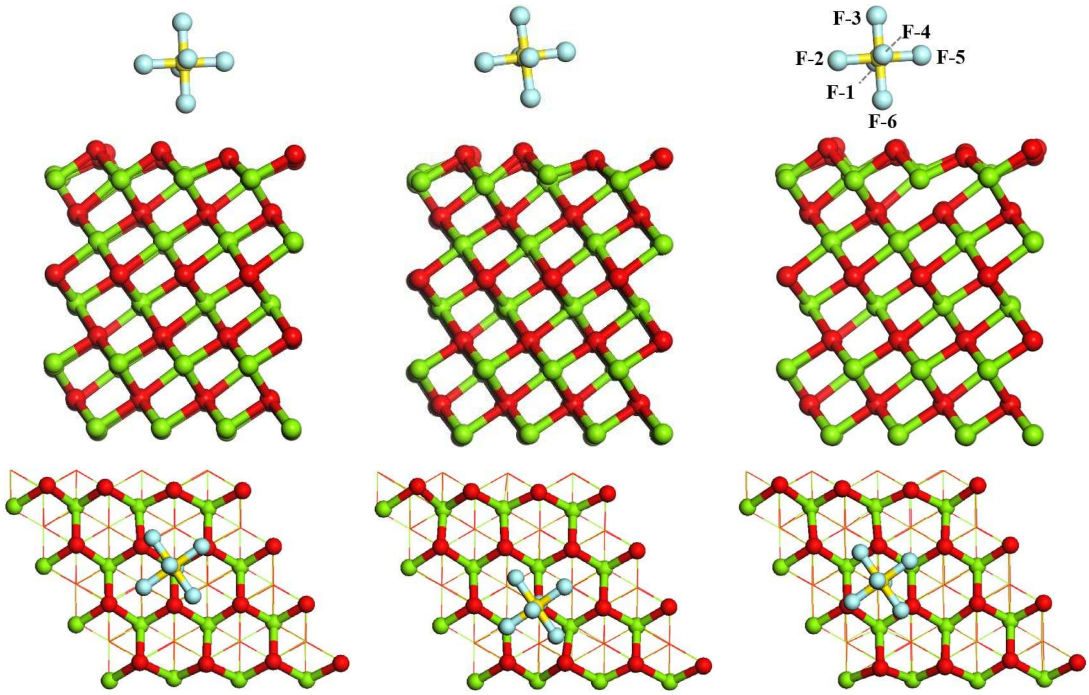

(a) Mg (b) O (c) Hollow

Fig. 2 Adsorption configurations of SF_6 over the perfect O-terminated MgO (111) surface, in side view (upper panels) and top view (lower panels). Green, red, yellow and blue balls are Mg, O, S and F atoms, respectively.

3.2 SF_6 adsorption over O-defective MgO (001) and (111) surfaces

Deficient MgO surfaces have been proven to show a better surface property than perfect surfaces for the adsorption and activation of gas molecules and doped atoms [28, 29]. In this study, the adsorption processes of SF_6 over O-defective MgO (001) and (111) surfaces are calculated. The E_{ad}, the adsorption distance and optimized configurations are summarized in Table 2, Fig.3 and Fig.4.

In Fig.3, SF_6 undergoes a chemical adsorption over the O-defective MgO (001) surface and the O_v site is the most stable site for SF_6 adsorption, corresponding to the highest E_{ad} of -6.66 eV. At this site, the SF_6 molecule decomposes to SF_5*(*means the species is adsorbed) and F*, where the F* atom fills the O vacancy, as shown in Fig.3(b). Similarly, at the bridge site, the SF_6 molecule decomposes to SF_5* and F*, with E_{ad} equal to -6.54 eV. However, at the Mg site, there is no decomposition of SF_6, but the bottom F in SF_6 binds with the surface Mg, with E_{ad} of -6.01 eV.

Table 2 Adsorption energy and distance of SF_6 over MgO (001) and MgO (111) surfaces with O vacancy

Adsorption site	MgO (001)		MgO (111)	
	E_{ad} (eV)	Adsorption distance[a] (Å)	E_{ad} (eV)	Adsorption distance[a] (Å)

Mg	-6.01	1.61	-0.22	2.74
O_v	-6.66	——	-0.58	——
Bridge	-6.54	——	——	——
Neighbor-O	——	——	-0.21	2.75

[a]This corresponds to the distance between the bottom F atom in SF_6 and the closest surface atom on the MgO surface.

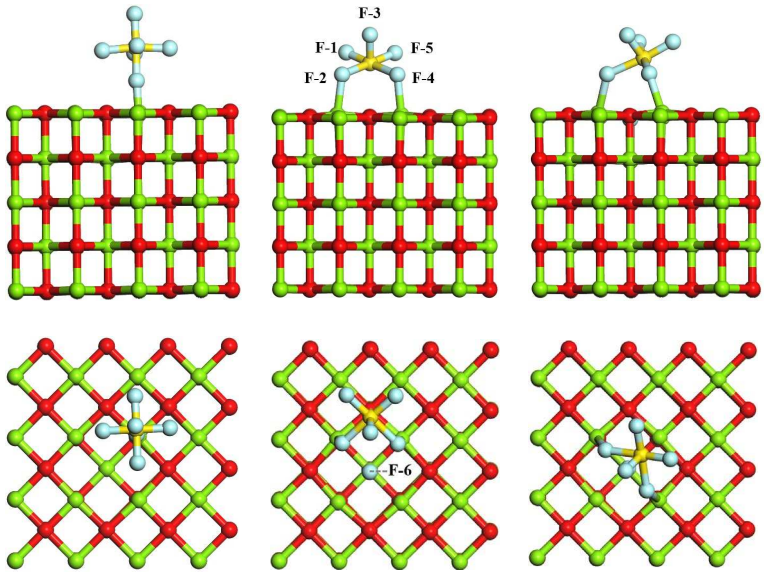

(a) Mg (b) O_v (c) Bridge

Fig. 3 Adsorption configurations of SF_6 over the MgO (001) surface with O vacancy, in side view (upper panels) and top view (lower panels). Green, red, yellow and blue balls are Mg, O, S and F atoms, respectively.

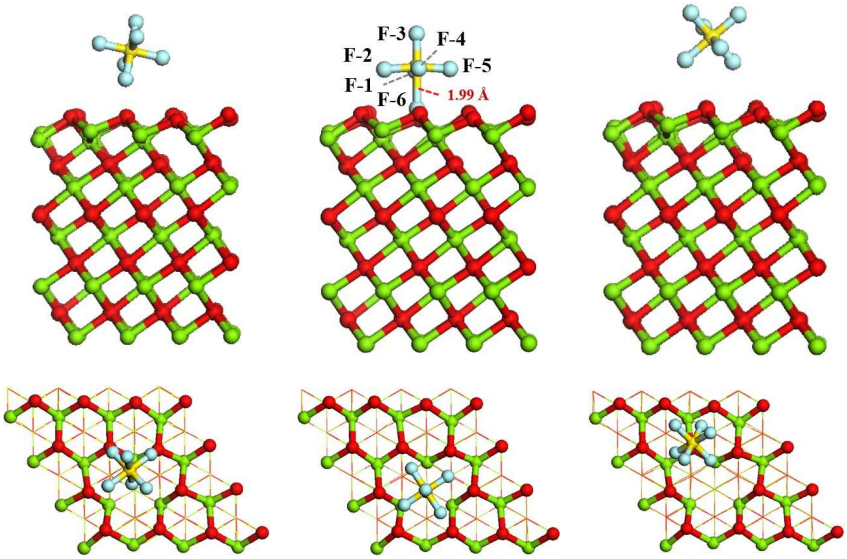

(a) Mg (b) O_v (c) Neighbor-O

Fig. 4 Adsorption configurations of SF_6 over the MgO (111) surface with O vacancy, in side view (upper panels) and top view (lower panels). Green, red, yellow and blue balls are Mg, O, S and F atoms, respectively.

By contrast, over the O-defective MgO (111) surface, E_{ad} is much lower. The O vacancy is also

the most stable site for SF_6 adsorption, corresponding to E_{ad} of -0.58 eV. Unlike the self-decomposition of SF_6 over the MgO (001) surface, the adsorption of SF_6 at the O_v site on the MgO (111) surface shows an elongation of the bottom S-F bond, from 1.61 Å to 1.99 Å (Fig.4(b)). On the other hand, in Fig.4 (a) and (c), the SF_6 molecule undergoes physical adsorption at both the Mg and neighboring O sites, corresponding to E_{ad} of -0.22 eV and -0.21 eV, respectively.

Table 3 Bader charge distributions of SF_6 in the gas phase, at the Mg site over the perfect MgO (001) surface, at the hollow site over the perfect MgO (111) and at the O_v site over the O-defective MgO (001) and (111) surfaces. (Unit: eV)

Atom	Gas phase	Mg site over the perfect MgO (001)	O_v site over the defective MgO (001)	Hollow site over the perfect MgO (111)	O_v site over the defective MgO (111)
S	0.00	0.00	2.52	0.00	0.00
F-1	8.01	8.02	7.99	8.01	8.18
F-2	7.99	8.00	7.68	8.02	8.03
F-3	7.99	7.98	8.12	7.99	8.01
F-4	8.01	8.02	7.68	8.01	8.05
F-5	8.00	8.00	8.00	7.99	8.02
F-6	8.00	8.04	7.96	7.96	7.74
Sum[a]	0	0.06	1.95	-0.02	0.03

[a]The total charge here is the value after subtracting the number of electrons in the valence layer of each atom of S and F (6 for S and 7 for F), which shows the overall charge change of the SF_6 molecule itself after the chemical reaction. Positive values indicate the gain of electrons. F atoms are labeled in Fig.1, Fig.2, Fig.3, and Fig.4.

In order to better understanding the interaction between SF_6 and the O-defective MgO surfaces, we calculated the Bader charge distributions and the partial charge distributions for the most stable adsorption configurations of the MgO (001) and (111) systems, as shown in Table 3 and Fig.5. For comparison, the Bader charges of two adsorption cases over the perfect MgO surfaces, as well as the gas-phase SF_6 molecule are calculated and summarized in Table 3 as well. From Table 3 we can see that SF_6 gains 1.95 |e| after its adsorption over the O-defective MgO (001) surface. In the SF_6 molecule, the S atom gains 2.52 |e|, while the F-2 and F-4 in Fig.3(b) lose 0.32 |e| each, which are two F atoms bonding with the surface Mg. This indicates that a strong electron transfer occurs during the adsorption, where SF_6 and surface MgO atoms act as the electron acceptor and donor, respectively, leading to a valence changing of the S and F atoms in SF_6. By comparison, the total charge transfer processes are very limited in other three adsorption cases, which are less than 0.1 |e|. However, from Table.3 and Fig.5(b) we can see that the F-6 (bottom F in SF_6) in the MgO (111) system loses 0.26 |e| after the SF_6 adsorption, which weakens the S-F bond and leads to S-F bond elongation. In general, the O-defective MgO (001) surface shows a significant surface property for SF_6 adsorption and activation, allowing SF_6 to decompose into SF_5* and F* over the surface during the adsorption. The adsorption of SF_6 over the O-defective MgO (111) surface is much weaker, but an elongation of the bottom S-F bond occurs, corresponding to a weaker activation of SF_6. This is in contract to the behavior at the perfect MgO surfaces, where the SF_6 molecule hardly interacts with the surface atoms and only physical adsorption happens.

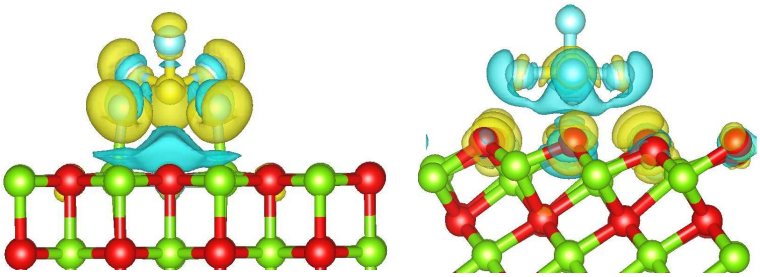

(a) MgO (001) (b) MgO (111)

Fig. 5 Differential charge distribution of SF_6 at the O_v site on the MgO(001) and (111) surfaces. The yellow region indicates an increase in charge density and the cyan region indicates a decrease.

3.3 SF_6 adsorption on the step-shape MgO (001) surface

The step site of the MgO surface could also be an active site for SF_6 adsorption [22]. As shown in Fig.6, the SF_6 molecule shows a deformation after adsorbing at the step site over the MgO (001) surface. The bond angle of F(2)-S-F(6) changes from 90° to 83.15° and the S-F(2) bond length increases from 1.61 Å to 1.99 Å. There is no obvious bonding process between SF_6 and surface atoms and the E_{ad} is -0.38 eV, which corresponds to physisorption.

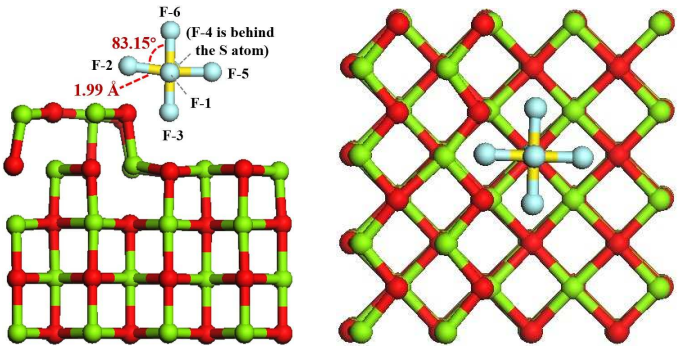

Fig. 6 Adsorption configurations of SF_6 over the step-shape MgO (001) surface, in side view (left) and top view (right). Green, red, yellow and blue balls are Mg, O, S and F atoms, respectively: E_{ad} = -0.38 eV.

Table 4 Bader charge distribution of SF_6 over the step-shape MgO (001) surface. (Unit: eV)

Atom*	Gas phase	Step site
S	0.00	0.00
F-1	8.01	7.96
F-2	7.99	7.99
F-3	7.99	8.14
F-4	8.01	8.03
F-5	8.00	7.97
F-6	8.00	8.04
Sum	0	0.13

*Positive values indicate the gain of electrons. F atoms are labeled in Fig.6.

The Bader charge distribution is shown in Table 4. The SF_6 molecule gains 0.13 |e| at the step site and the charge transfer mainly happens between SF_6 and the step O atoms, which is also proved by the charge density difference in Fig.7. The projected density of state (PDOS) is analyzed to further study the orbital interactions between the SF_6 molecule and the step O atoms, as shown in Fig.8. The PDOS results show that there is a small overlap between the F atoms and the step O atoms at

about -1 eV, which may correspond to a very weak orbital hybridization. Overall, SF_6 mainly undergoes physisorption at the step site over the MgO (001) surface, with a weak charge transfer process. The step-shape MgO (001) weakly activates SF_6, leading to a limited elongation of the S-F bond and a change in S-F bond angles.

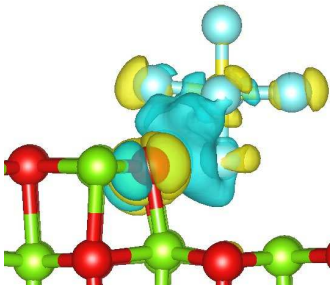

Fig.7 Differential charge distribution of SF_6 over the step-shape MgO (001) surface. The yellow region indicates an increase in charge density and the cyan region indicates a decrease.

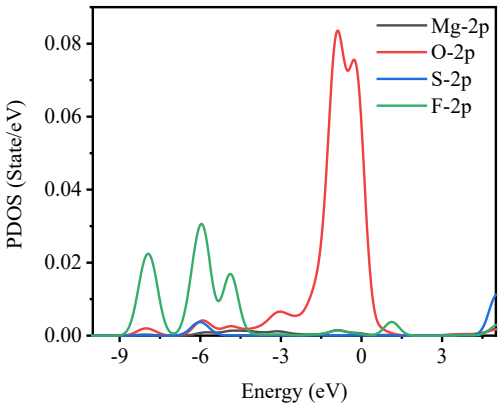

Fig. 8 PDOS for SF_6 adsorption over step-shape MgO (001) surface

3.4 SF_6 adsorption over H-covered MgO (111) surfaces

As previously mentioned, the terminated MgO surfaces should be carefully evaluated since the hydration process may occur in SF_6 degradation with H_2O or H_2 addition. The hydroxylated MgO (111) surfaces has been proven to be more stable than clean (100) surfaces [30]. Therefore, in this study, we chose the hydroxylated MgO (111) surface as a typical case to represent the possible surface condition of MgO in thermal or NTP treatment and investigate its surface properties on SF_6 adsorption. Two hydroxylated conditions are set, namely 0.5 ML and 1.0 ML coverage of H for the MgO (111) surface, as shown in Fig. S3. The E_{ad} and adsorption configurations are summarized in Table 5, Fig.9 and Fig.10.

In Table 5, the E_{ad} of SF_6 in the 0.5 ML H-covered MgO (111) system is significantly lower than in the 1.0 ML system. As shown in Fig.9, at each site, SF_6 undergoes physisorption over the 0.5 ML surface without a surface binding process and E_{ad} is no more than 0.20 eV. By contrast, over the 1.0 ML H-covered (111) surface, SF_6 shows a significant deformation after the adsorption at the four typical sites. The H site is the most stable site, at which SF_6 decomposes to SF_5 and F after the adsorption, corresponding to E_{ad} of -4.22 eV. In Fig.10 (b), the detached F atom (F-5) is at the hollow site. Similarly, SF_6 decomposes at the hollow site and the bridge site, corresponding to E_{ad} of -4.05 eV and -4.14 eV, respectively. However, at the Mg site, there is no obvious detachment of F in SF_6,

but an elongation of the bottom S-F bond from 1.61 Å to 2.07 Å is seen. The adsorption configurations in Fig.9 and Fig.10 show that the adsorption of SF_6 is much more stable at the 1.0 ML H-covered (111) surface.

Table 5 Adsorption energy of SF_6 over the O-terminated MgO (111) surface with 0.5 and 1.0 ML H-coverage (Unit: eV)

Adsorption site	0.5 ML	1.0 ML
H	-0.17	-4.22
O	-0.04	——
Mg	——	-3.13
hollow	-0.20	-4.05
bridge	-0.12	-4.14

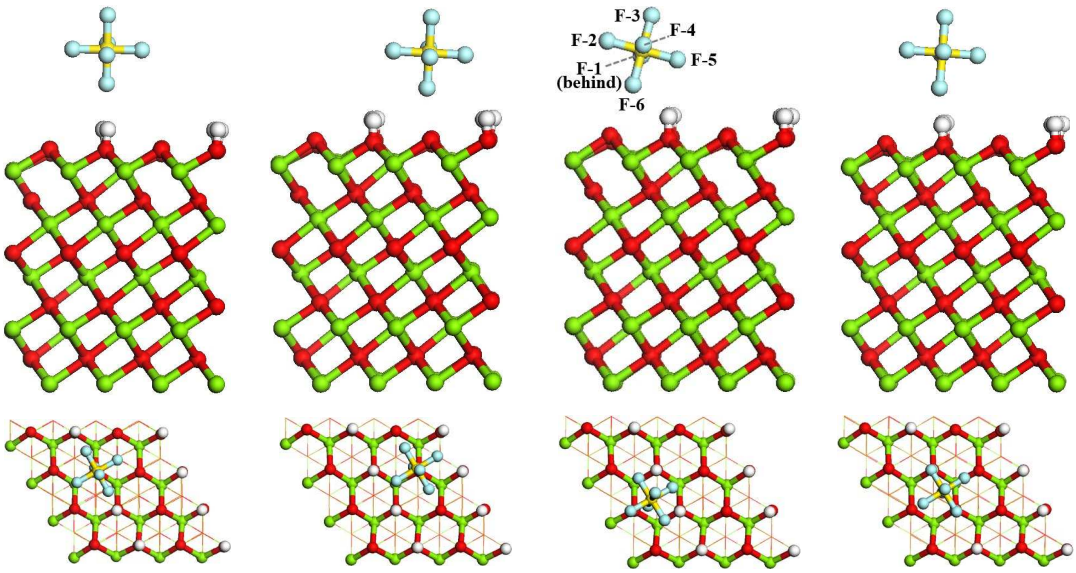

(a) H (b) O (c) Hollow (d) Brigde

Fig. 9 Adsorption configurations of SF_6 over the MgO (111) surface with 0.5 ML H-coverage, in side view (upper panels) and top view (lower panels). Green, red, white, yellow and blue balls are Mg, O, H, S and F atoms, respectively.

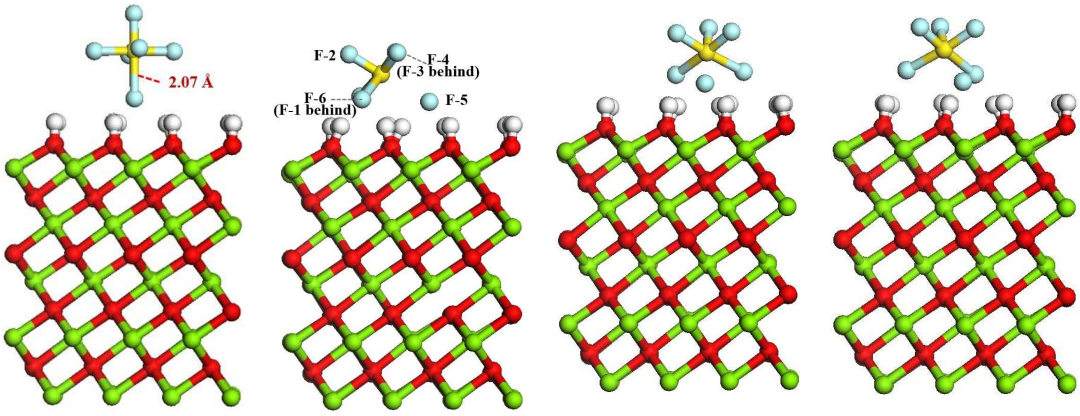

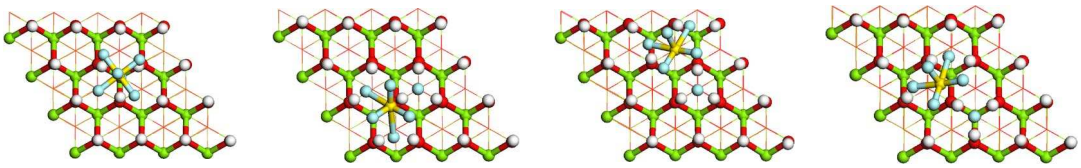

(a) Mg (b) H (d) Hollow (c) Brigde

Fig. 10 Adsorption configurations of SF_6 over the MgO (111) surface with 1.0 ML H-coverage, in side view (upper panels) and top view (lower panels). Green, red, yellow and blue balls are Mg, O, S and F atoms, respectively.

Bader analysis and partial charge calculation are conducted for two hydroxylated adsorption systems, as shown in Table 6 and Fig.11. It can be seen that the S atom in SF_6 gains 2.34 |e| from the 1.0 ML H-covered (111) surface, while it stays unchanged at the 0.5 ML surface. The SF_6 molecule gains 0.02 and 1.92 |e| from the 0.5 ML and 1.0 ML surfaces, respectively. This indicates that there is almost no charge transfer process in the 0.5 ML adsorption system but a significant transfer of electrons happens from the 1.0 ML surface to the SF_6 molecule, leading to a change of the valence state of the S atom. Similar to the adsorption of SF_6 over the O-defective (111) surface, the bottom three F atoms, i.e. F-1, F-5 and F-6 lose -0.32, -0.26 and -0.28 |e|, respectively, which is also proven in Fig.11 (b). Finally, from Fig.11 (a) we can see that the partial charge distribution of SF_6 hardly changes over the 0.5 ML (111) surface.

Table 6 Bader charge distribution of SF_6 on the 0.5 ML and the 1.0 ML H-coverage MgO (111) surface. (Unit: eV)

Atom*	Gas phase	0.5 ML Hollow site	1.0 ML H site
S	0.00	0.00	2.34
F-1	8.01	8.01	7.68
F-2	7.99	7.98	8.07
F-3	7.99	8.01	8.07
F-4	8.01	8.00	8.00
F-5	8.00	7.99	7.74
F-6	8.00	8.03	7.72
Sum	0	0.02	1.92

*Positive values indicate the gain of electrons. F atoms are labeled in Fig.9 and Fig.10.

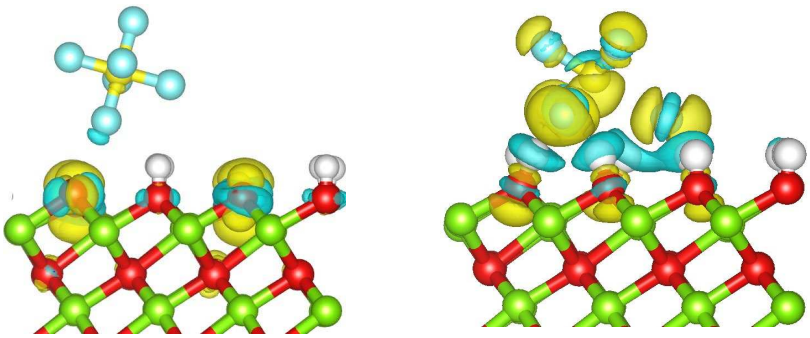

(a) Hollow site with 0.5 ML H-coverage (b) H site with 1.0 ML H-coverage

Fig.11 Differential charge distribution of SF_6 at the H-covered MgO (111) surfaces. The yellow region indicates an increase in charge density and the cyan region indicates a decrease.

In order to further analyze the bonding properties of the SF_6 molecule and the surface atoms, PDOS analysis is carried out for two adsorption systems, as shown in Fig.12. The PDOS results of O correspond to the surface O atoms. In Fig.12 (a) of the 0.5 ML system, there is no obvious overlap

between the orbitals of the surface atoms and SF_6. However, in Fig.12 (b) of the 1.0 ML system, the F-1p overlaps with O-1p at around -1.7 eV and -0.8 eV. The S-2p and F-1p overlap with O-1p and H-1s at around -3.3 eV. This corresponds to the orbital hybridization of SF_6 and the surface atoms, which indicates that the detached and elongated F atoms from SF_6 show a chemical bonding process with the surface atoms, accompanied with a charge transfer from the surface slab to the gas molecule. In general, the 1.0 ML H-covered (111) surface shows significant surface properties for SF_6 adsorption and activation, which can promote the decomposition of SF_6 to stable adsorbates on its surface. However, over the 0.5 ML surface, only physisorption of SF_6 occurs.

Overall, the adsorption performance of SF_6 over the MgO surface is largely determined by the surface properties. The crystal type, surface defect, crystal surface shape (step site) and the surface hydroxylation are analyzed to be potential factors in affecting SF_6 adsorption and activation. Among them, O vacancies and surface hydroxylation of O-terminated (111) surface can both lead to the initial bond-breaking of SF_6 and the chemical adsorption of its decompositions, which could promote the degradation of SF_6. It should be noted that in a plasma-catalysis system, the intensive discharges generated at the gas-solid (catalyst) interface can significantly change the surface structure of the catalyst, leading to the formation of surface vacancies and the pre-adsorption of plasma-generated species [10, 11]. Therefore, when packing the MgO into a plasma system for SF_6 degradation, the surface O vacancies and surface hydroxylation are likely to be formed by the plasma discharge, especially with the addition of H_2O or H_2 gas. In this case, the adsorption and activation of SF_6 could be promoted over the MgO packing surface to obtain a better degradation performance. To fully understand the complete picture of SF_6 degradation in a MgO packed system, in-situ characterization of the plasma-assisted abatement of SF_6 can be considered in the future, and more detailed elementary reactions could be calculated when advanced product information is known.

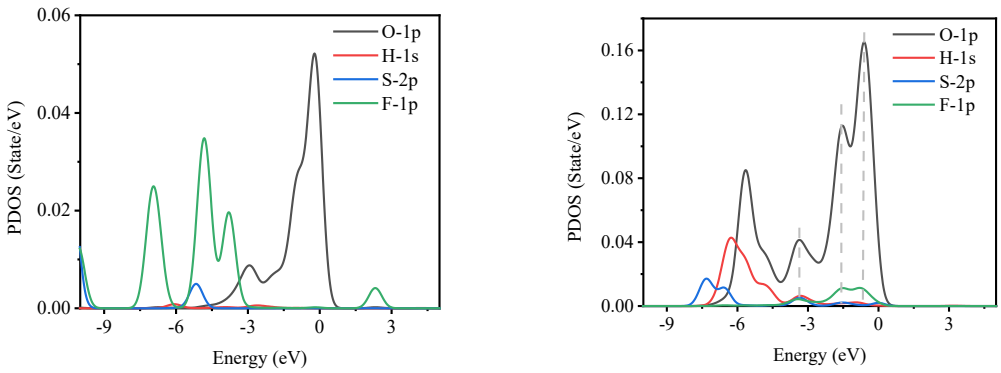

(a) Hollow site with 0.5 ML H-coverage (b) H site with 1.0 ML H-coverage

Fig. 12 Project DOS for SF_6 adsorption over the H-covered MgO (111) surfaces

4 Conclusion

In this study, the interaction mechanism between SF_6 and MgO surfaces are investigated via DFT calculations. Our results show that the crystal surface type and the surface structures are of great importance in determining the surface properties on SF_6 adsorption and activation. Over perfect MgO (001) and (111) surfaces, SF_6 only undergoes physisorption without bonding. By contrast, SF_6 undergoes chemisorption over O-defective MgO (001) surface, with the highest E_{ad} to be -6.66 eV, and SF_6 decomposes to SF_5* and F* after adsorption. Besides, SF_6 undergoes adsorption at the O_v

site over the (111) surface with E_{ad} to be -0.58 eV, accompanied with an elongation of the bottom S-F bond from 1.61 Å to 1.99 Å. Bader analysis shows that 1.95 |e| electrons are transferred from the O-defective (001) surface to SF_6, leading to a change of valence state of the S atom in SF_6 and a weakening of the S-F bonds. In the O-defective (111) system, the total charge transfer is very limited, but the bottom F atom loses 0.26 |e|, which is attributed to the S-F bond elongation.

Besides, over the step-shape (001) surface, SF_6 shows physisorption at the stepsite with E_{ad} to be -0.38 eV. It is slightly activated as the S-F bond angles are changed and the bond lengths are elongated. A weak charge transfer process accompanied by a weak hybridization process occurs during the adsorption.

Moreover, as hydroxylated MgO (111) surface we considered two examples, i.e., a 0.5 ML and 1.0 ML H-covered O-terminated (111) surface. The results show that SF_6 can undergo chemisorption on the 1.0 ML H-covered (111) surface, but physisorption on the 0.5 ML surface. On the 1.0 ML H-covered surface, the H site is the most stable site, corresponding to the highest E_{ad} of -4.22 eV, at which 1.92 |e| is transferred from the MgO surface to SF_6 and a significant orbital interaction occurs between SF_6 and the surface atoms. By contrast, there is almost no charge transfer or orbital hybridization process in the 0.5 ML H-covered system.

Overall, our results prove that the MgO surface shows potential for SF_6 adsorption and activation when the surface is O defective or is hydroxylated. At these conditions, SF_6 can undergo self-decomposition during the adsorption, accompanied with significant charge transfer and surface bonding. Therefore, when using a packed bed DBD with MgO packing in NTP-based degradation of SF_6, and the plasma affects the MgO surface, the latter can obtain catalytic properties for SF_6 degradation. Hence, our results can be useful to obtain more insight in the activation and initial degradation mechanisms of SF_6 in plasma-catalytic treatment with MgO packing.

ACKNOWLEDGMENT

This work is funded by National Natural Science Foundation of China (Grant. 52207155). The computational resources and services used in this work were provided by the HPC core facility CalcUA of the Universiteit Antwerpen, and VSC (Flemish Supercomputer Center), funded by the Research Foundation - Flanders (FWO) and the Flemish Government.

REFERENCES

[1] Christophorou L G, Olthoff J K, Van Brunt R J. Sulfur hexafluoride and the electric power industry [J]. IEEE Electrical Insulation Magazine, 1997, 13(5): 20-24.

[2] Reilly J, Prinn R, Harnisch J, et al. Multi-gas assessment of the Kyoto Protocol [J]. Nature, 1999, 401(6753): 549-555.

[3] Dervos C T, Vassiliou P. Sulfur hexafluoride (SF_6): global environmental effects and toxic byproduct formation [J]. Journal of the Air & Waste Management Association, 2000, 50(1): 137-141.

[4] Kashiwagi D, Takai A, Takubo T, et al. Catalytic activity of rare earth phosphates for SF_6 decomposition and promotion effects of rare earths added into $AlPO_4$[J]. Journal of colloid and interface science, 2009, 332(1): 136-144.

[5] Zhang J, Zhou J Z, Liu Q, et al. Efficient removal of sulfur hexafluoride (SF_6) through reacting with recycled electroplating sludge [J]. Environmental science & technology, 2013, 47(12): 6493-6499.

[6] Zhang X, Xiao H, Tang J, et al. Recent advances in decomposition of the most potent greenhouse gas SF_6[J]. Critical Reviews in Environmental Science and Technology, 2017,

47(18): 1763-1782.
[7] Lee H, Chang M, Wu K. Abatement of sulfur hexafluoride emissions from the semiconductor manufacturing process by atmospheric-pressure plasmas [J]. Journal of the Air & Waste Management Association, 2004, 54(8): 960-970.
[8] Cui Z, Zhang X, Yuan T, et al. Plasma-assisted abatement of SF_6 in a dielectric barrier discharge reactor: investigation of the effect of packing materials[J]. Journal of Physics D: Applied Physics, 2019, 53(2): 025205.
[9] Gutierrez Y, Giangregorio M M, Palumbo F, et al. Sustainable and Tunable Mg/MgO Plasmon-Catalytic Platform for the Grand Challenge of SF_6 Environmental Remediation[J]. Nano Letters, 2020, 20(5): 3352-3360.
[10] Bogaerts A, Tu X, Whitehead J C, et al. The 2020 plasma catalysis roadmap[J]. Journal of physics D: applied physics, 2020, 53(44): 443001.
[11] Neyts E C, Ostrikov K, Sunkara M K, et al. Plasma catalysis: synergistic effects at the nanoscale[J]. Chemical reviews, 2015, 115(24): 13408-13446.
[12] Zhang X, Cui Z, Li Y, et al. Abatement of SF_6 in the presence of NH_3 by dielectric barrier discharge plasma[J]. Journal of hazardous materials, 2018, 360: 341-348.
[13] Zhang X, Yuan T, Cui Z, et al. Plasma-assisted abatement of SF_6 in a packed bed plasma reactor: understanding the effect of gas composition[J]. Plasma Science and Technology, 2020, 22(5): 055502.
[14] Finocchi F, Barbier A, Jupille J, et al. Stability of rocksalt (111) polar surfaces: Beyond the octopole[J]. Physical Review Letters, 2004, 92(13): 136101.
[15] Cadigan C A, Corpuz A R, Lin F, et al. Nanoscale (111) faceted rock-salt metal oxides in catalysis[J]. Catalysis Science & Technology, 2013, 3(4): 900-911.
[16] Gibson A, Haydock R, LaFemina J P. Electronic structure and relative stability of the MgO (001) and (111) surfaces[J]. Journal of Vacuum Science & Technology A: Vacuum, Surfaces, and Films, 1992, 10(4): 2361-2366.
[17] Zhang W B, Tang B Y. Stability of MgO (111) polar surface: Effect of the environment[J]. The Journal of Physical Chemistry C, 2008, 112(9): 3327-3333.
[18] Hutter J, Iannuzzi M, Schiffmann F, et al. cp2k: atomistic simulations of condensed matter systems [J]. Wiley Interdisciplinary Reviews: Computational Molecular Science, 2014, 4(1): 15-25.
[19] Perdew J, Burke K, Ernzerhof M. Generalized gradient approximation made simple [J]. Physical review letters, 1996, 77(18): 3865.
[20] Grimme S, Antony J, Ehrlich S, et al. A consistent and accurate ab initio parametrization of density functional dispersion correction (DFT-D) for the 94 elements H-Pu [J]. The Journal of chemical physics, 2010, 132(15): 154104.
[21] Goedecker S, Teter M, Hutter J. Separable dual-space Gaussian pseudopotentials [J]. Physical Review B, 1996, 54(3): 1703.
[22] VandeVondele J, Hutter J. Gaussian basis sets for accurate calculations on molecular systems in gas and condensed phases [J]. The Journal of chemical physics, 2007, 127(11): 114105.
[23] Henkelman G, Arnaldsson A, Jónsson H. A fast and robust algorithm for Bader decomposition of charge density [J]. Computational Materials Science, 2006, 36(3): 354-360.
[24] Richter N A, Sicolo S, Levchenko S V, et al. Concentration of vacancies at metal-oxide surfaces: Case study of MgO (100)[J]. Physical review letters, 2013, 111(4): 045502.
[25] Hao Y, Liu B, Tian L, et al. Synthesis of {111} facet-exposed MgO with surface oxygen vacancies for reactive oxygen species generation in the dark[J]. ACS applied materials & interfaces, 2017, 9(14): 12687-12693.
[26] Wang H, Zhong C, Ma Q, et al. The adsorption and oxidation of SO_2 on MgO surface: experimental and DFT calculation studies[J]. Environmental Science: Nano, 2020, 7(4): 1092-1101.

[27] Mutch G A, Shulda S, McCue A J, et al. Carbon capture by metal oxides: Unleashing the potential of the (111) facet[J]. Journal of the American Chemical Society, 2018, 140(13): 4736-4742.
[28] Yang Z, Wu R, Zhang Q, et al. Adsorption of Au on an O-deficient MgO (001) surface[J]. Physical Review B, 2002, 65(15): 155407.
[29] Florez E, Fuentealba P, Mondragón F. Chemical reactivity of oxygen vacancies on the MgO surface: Reactions with CO_2, NO_2 and metals[J]. Catalysis today, 2008, 133: 216-222.
[30] Wander A, Bush I J, Harrison N M. Stability of rocksalt polar surfaces: An ab initio study of MgO (111) and NiO (111)[J]. Physical Review B, 2003, 68(23): 233405.

Theoretical study of SF_6 adsorption and decomposition over the MgO (001) and (111) surfaces

Zhaolun Cui[a,b], Yanpeng Hao[a], Amin Jafarzade[b], Shangkun L[b], Annemie Bogaerts[b], Licheng Li[a]*

[a]School of Electric Power Engineering, South China University of Technology, Guangzhou 510630, China

[b]Research group PLASMANT, Department of Chemistry, University of Antwerp, Universiteitsplein 1, BE-2610 Wilrijk-Antwerp, Belgium

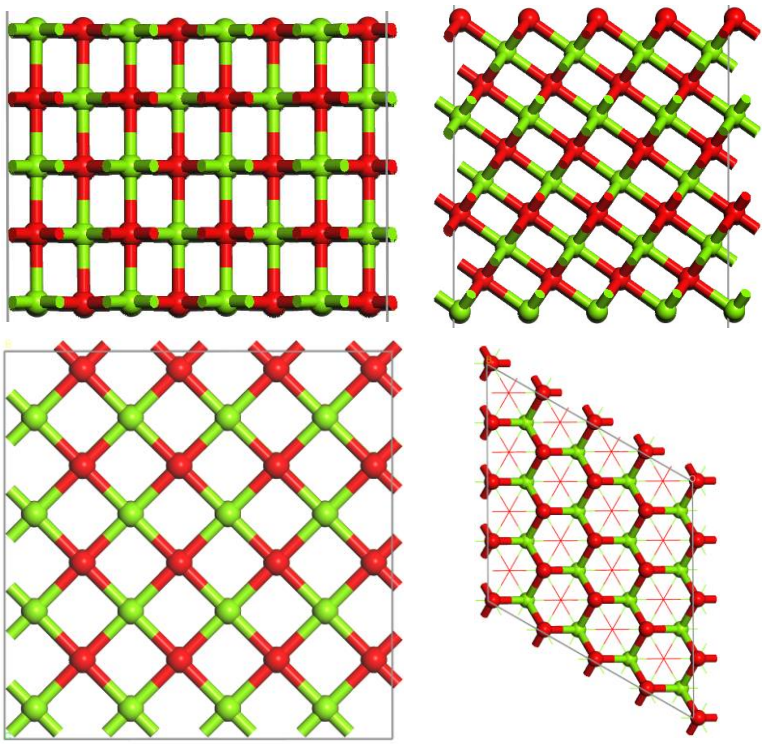

(a) MgO (001) (b) MgO (111)

Fig.S1 Bulk models of the perfect MgO (001) (a) and O-terminated (111) (b) slabs, in side view (upper panels) and top view (lower panels). Green and red balls are Mg and O atoms, respectively.

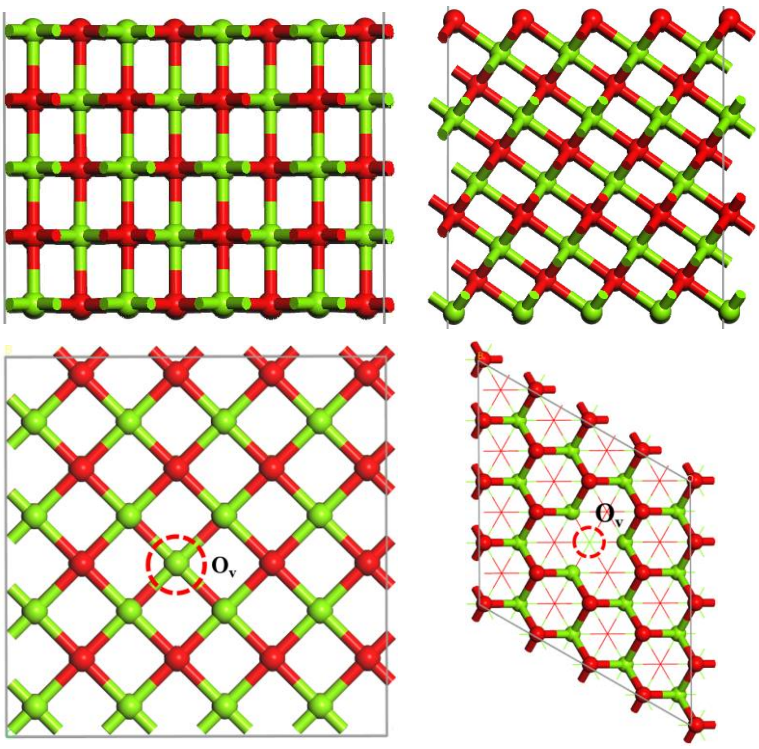

(a) MgO (001) (b) MgO (111)

Fig.S2 Bulk models of the MgO (001) (a) and O-terminated (111) slabs (b) with one O vacancy (O_v), in side view (upper panels) and top view (lower panels). Green and red balls are Mg and O atoms, respectively.

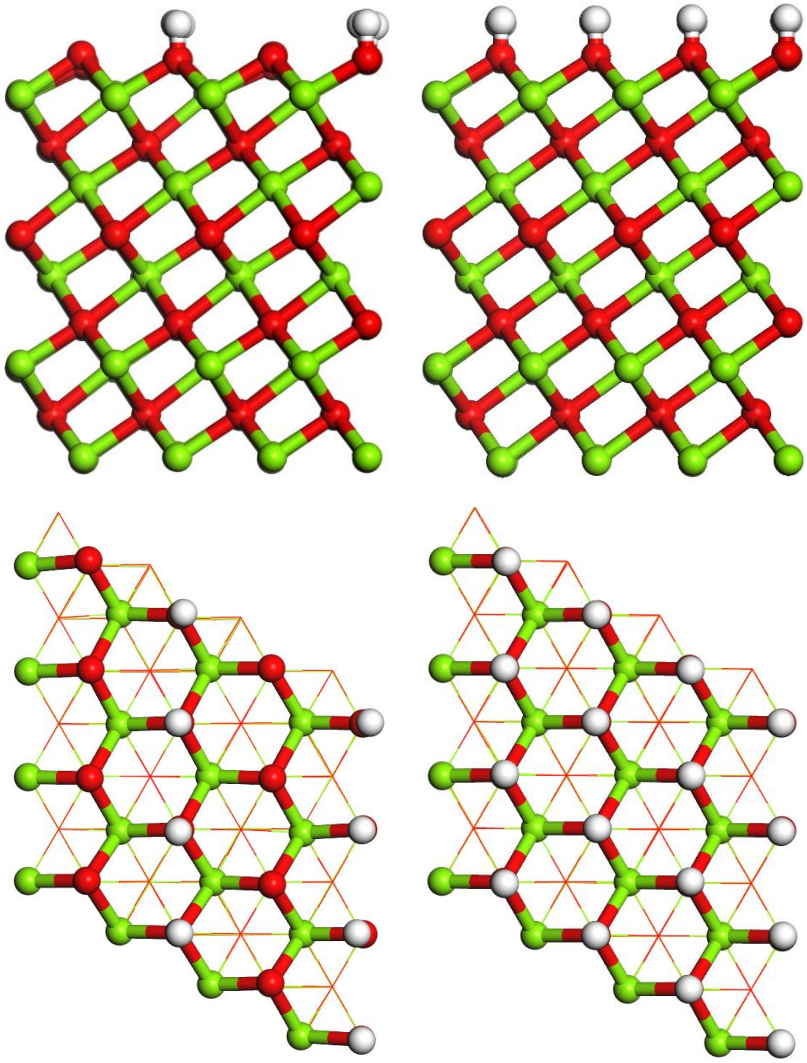

(a) 0.5 ML (b) 1.0 ML

Fig.S3 Bulk models of the O-terminated (111) slabs with 0.5 (a) and 1.0 ML (b) H-coverage, in side view (upper panels) and top view (lower panels). Green, red and white balls are Mg, O and H atoms, respectively.